Supporting Information
for

Scalable Synthesis of High-quality Transition Metal Dichalcogenide Nanosheets and Their Application as Sodium-Ion Battery Anodes

Jingwen Zhou [a], Jian Qin [a], Lichao Guo [a], Naiqin Zhao [ab], Chunsheng Shi [a], Enzuo Liu [a,b], Fang He[a] , Liying Ma[a], Jiajun Li [a] and Chunnian He *[ab]

[a] *School of Materials Science and Engineering and Tianjin Key Laboratory of Composites and Functional Materials, Tianjin University, Tianjin 300072, China.*

**E-mail: cnhe08@tju.edu.cn*

[b] *Collaborative Innovation Center of Chemical Science and Engineering, Tianjin 300072, China*

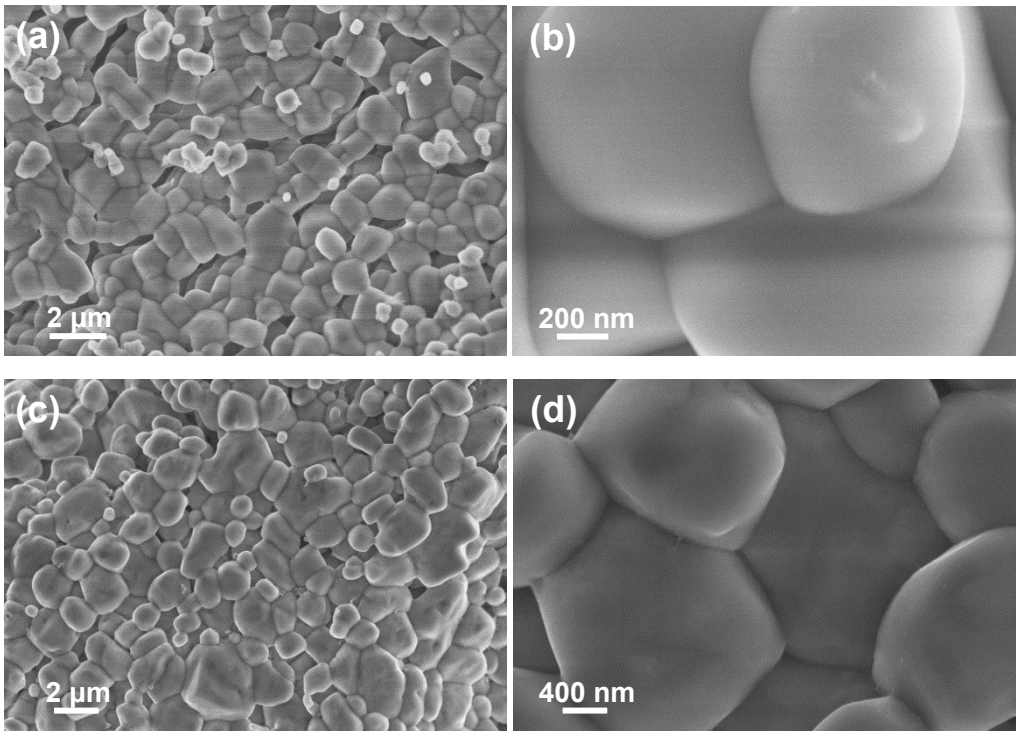

Figure S1. (a)-(b) Typical SEM images of the freeze-dried precursor gel consisting of NH_2CSNH_2-$(NH_4)_6W_{12}O_{39}$-NaCl, revealing that 3D NaCl self-assembly was covered with the discontinuous thin films of NH_2CSNH_2-$(NH_4)_6W_{12}O_{39}$ complex during the freeze-drying process. (c)-(d) SEM images of these NaCl cubes coated with WS_2 nanosheets before washing away the templates, indicating that the 3D assembly was well preserved after the calcination process and WS_2 nanosheets were formed between the surfaces of adjacent NaCl particles.

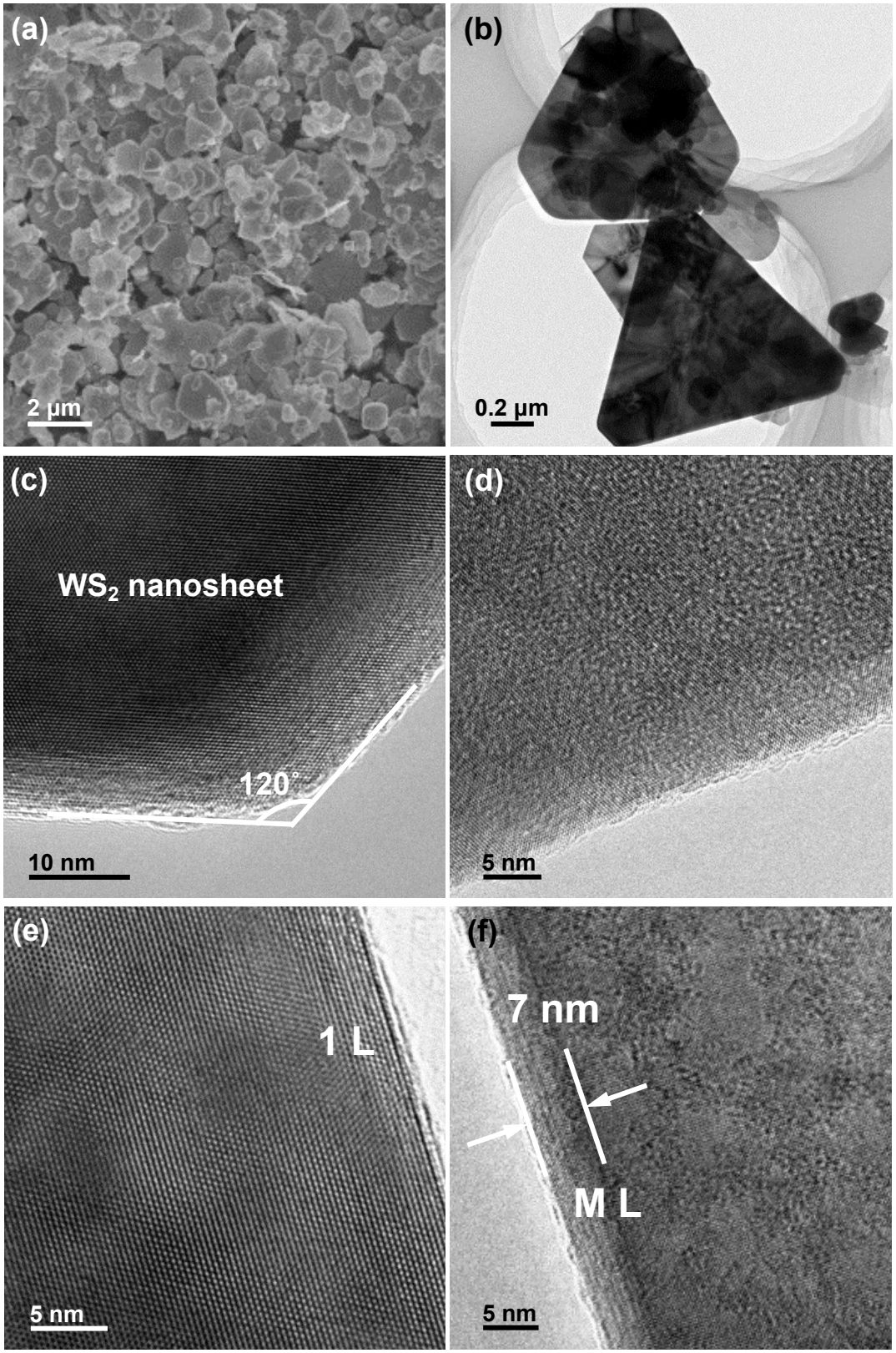
(a)
2 μm
(b)
0.2 μm
(c)
WS2 nanosheet
120˚
10 nm
(d)
5 nm
(e)
1 L
5 nm
(f)
7 nm
M L
5 nm

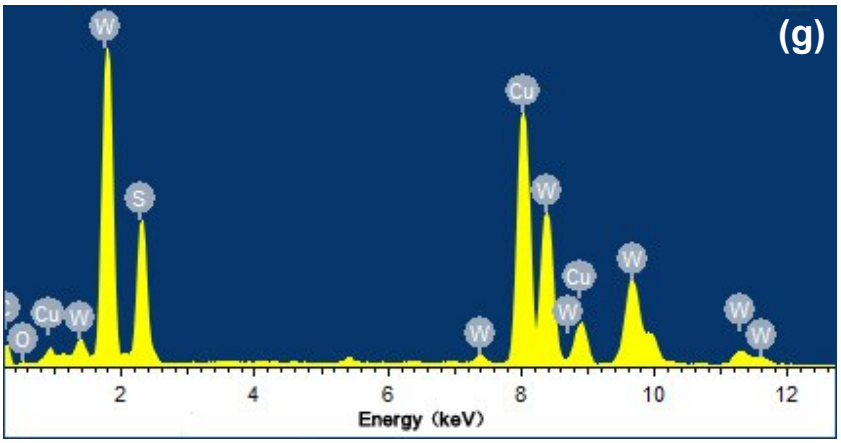

Figure S2. (a) Low-magnified SEM image of the as-synthesized WS_2 nanosheets. (b)-(d) TEM images of the as-synthesized WS_2 nanosheets. (e) HRTEM image of the WS_2 nanosheets obtained from an experiment of higher ratio of NaCl to WS_2 precursor. (f) HRTEM image of the WS_2 nanosheets obtained from an experiment of lower ratio of NaCl to WS_2 precursor. (g) EDX spectrum of a specific area in which some typical WS_2 nanosheets were displayed.

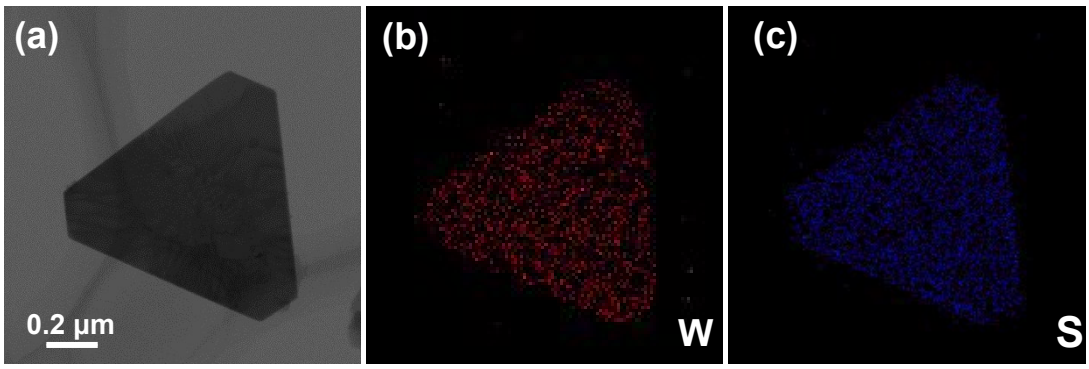

Figure S3. (a) STEM image of an individual WS_2 nanosheet. (b) EDX element mapping of W and (c) EDX element mapping of S corresponding to the area in STEM image of (a).

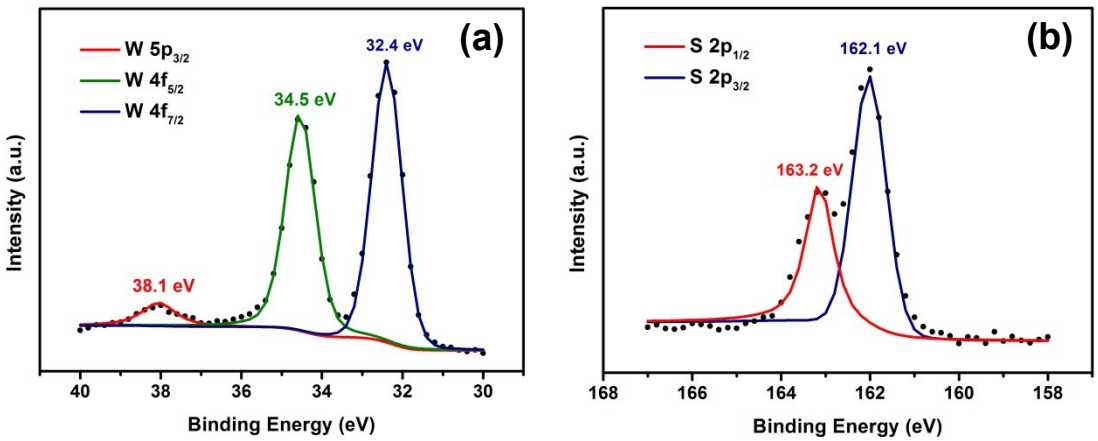

Figure S4. XPS spectra of the as-synthesized WS_2 nanosheets: (a) W4f and W5p peaks, and (b) S2p peaks.

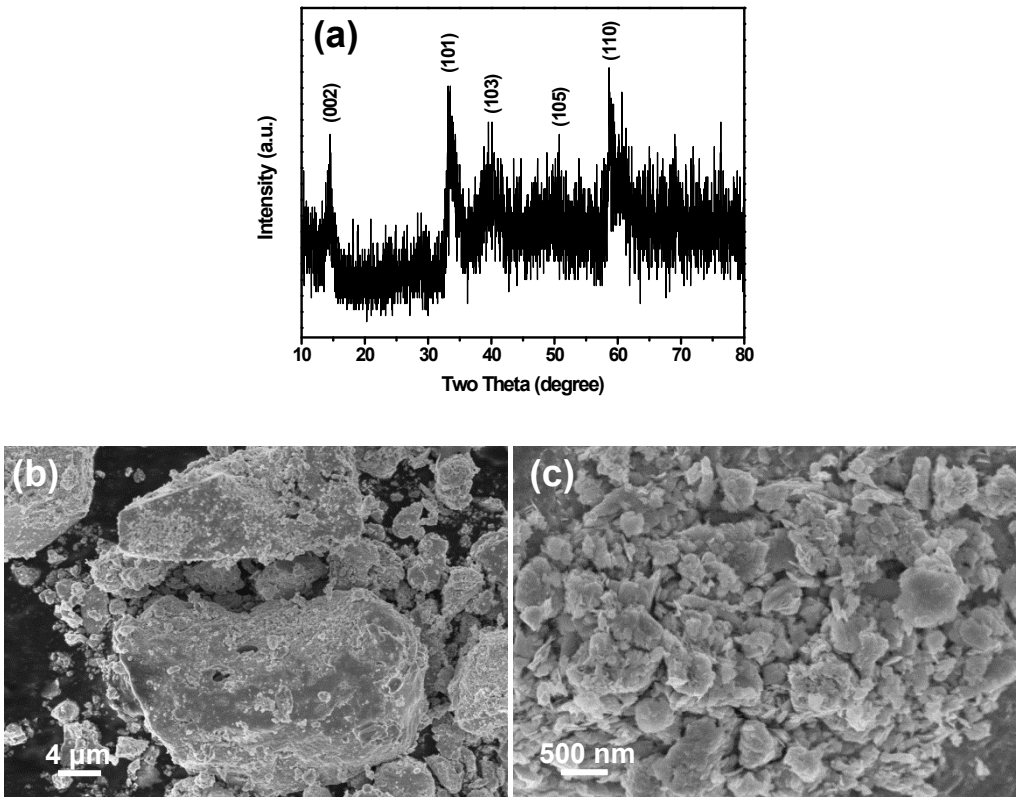

Figure S5. (a) XRD pattern and (b) Low-magnified SEM image of these disordered WS_2 blocks synthesized by CVD technique. (c) FE-SEM image of the surface of a typical WS_2 block.

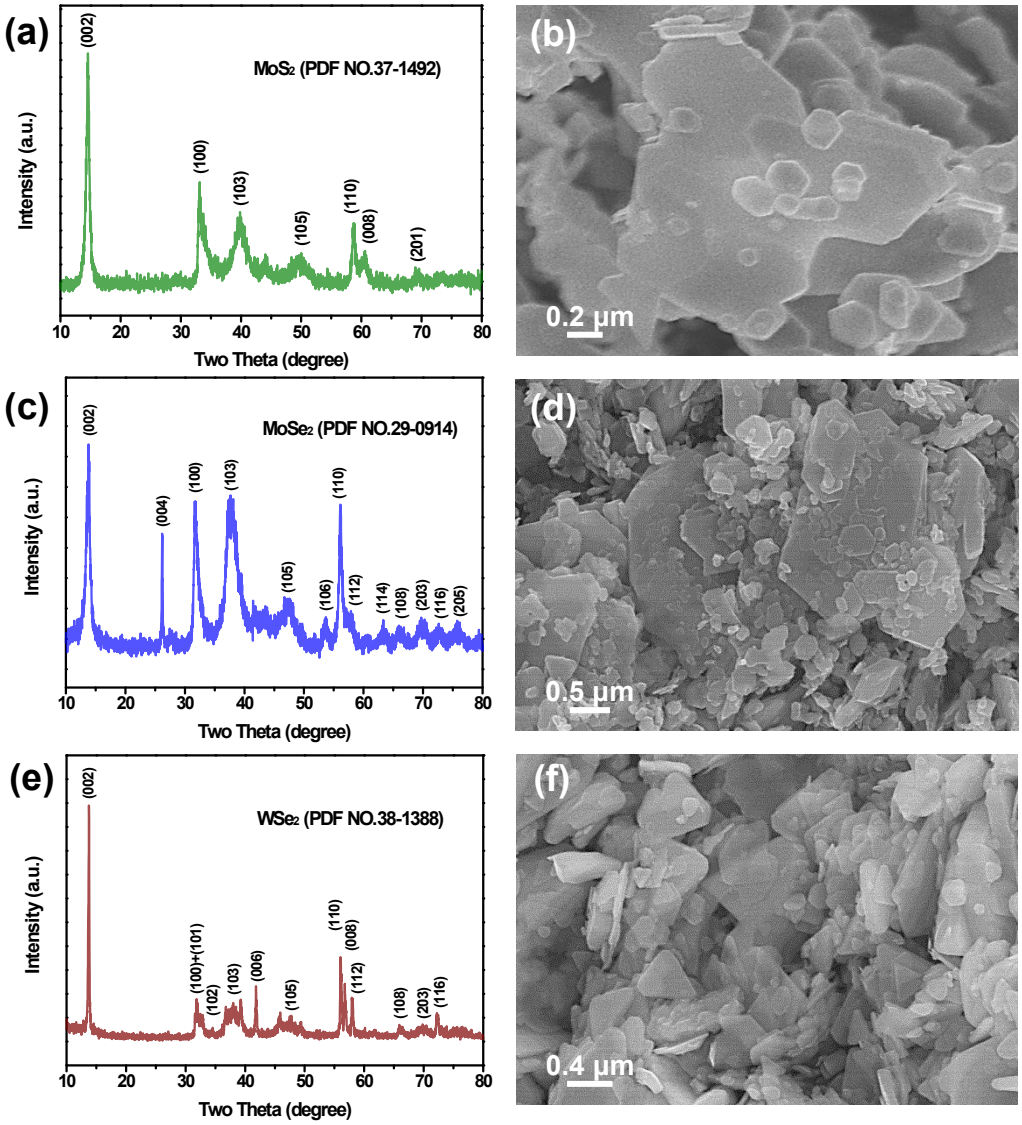

Figure S6. XRD patterns and typical SEM images of the TMD nanosheets produced through the facile NaCl template-assisted CVD strategy: (a)(b) MoS_2, (c)(d) $MoSe_2$ and (e)(f) WSe_2, respectively.

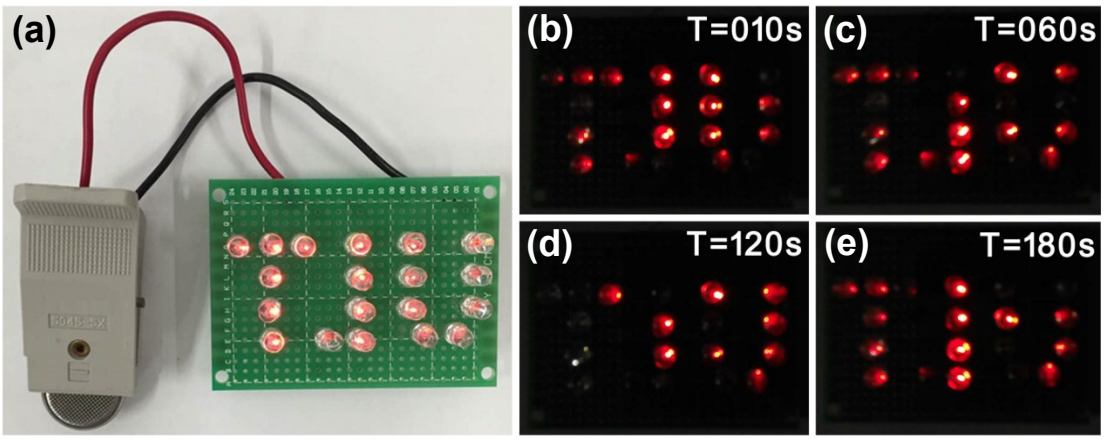

Figure S7. (a) The photo illustrating a light-emitting diode application of the sodium-ion battery cell even after 60 cycles at 0.1 A g^{-1}, where the as-synthesized WS_2 nanosheets coated Cu foil act as the working anode. Photos of the nineteen randomly twinkling light-emitting diodes at different times of (b) T=10s, (c) T=60s, (d) T=120s and (e) T=180s, respectively.

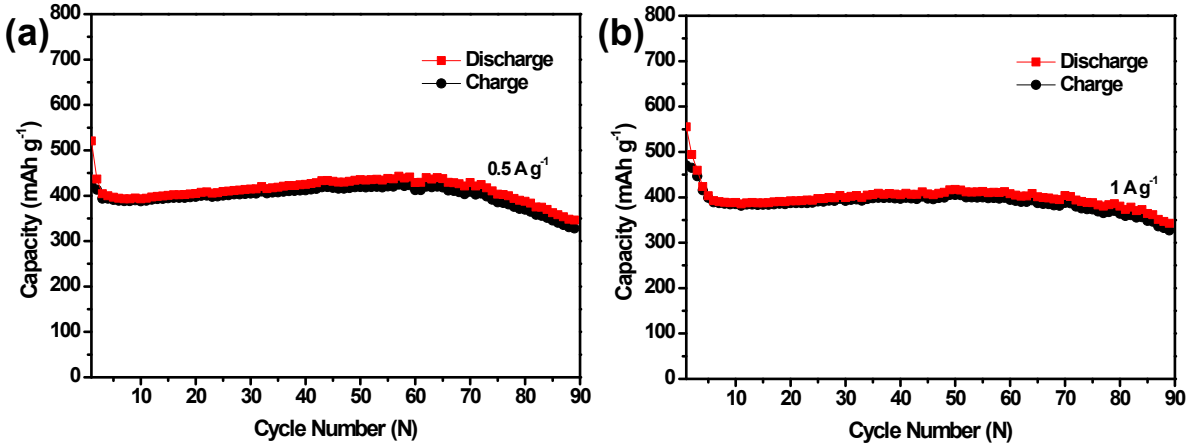

Figure S8. Cycling performance of WS_2 nanosheets electrodes at a current density of (a) 0.5 A g^{-1} and (b) 1 A g^{-1} for sodium-ion batteries, respectively.

Table S2. Kinetic parameters of the electrodes of WS_2 nanosheets and WS_2 blocks after the rate capability test obtained by fitting the EIS curves based on the corresponding equivalent circuit.

Samples	R_e **(Ω)**	R_{ct} **(Ω)**
WS_2 nanosheets	5.74	80.6
WS_2 blocks	4.90	203.7

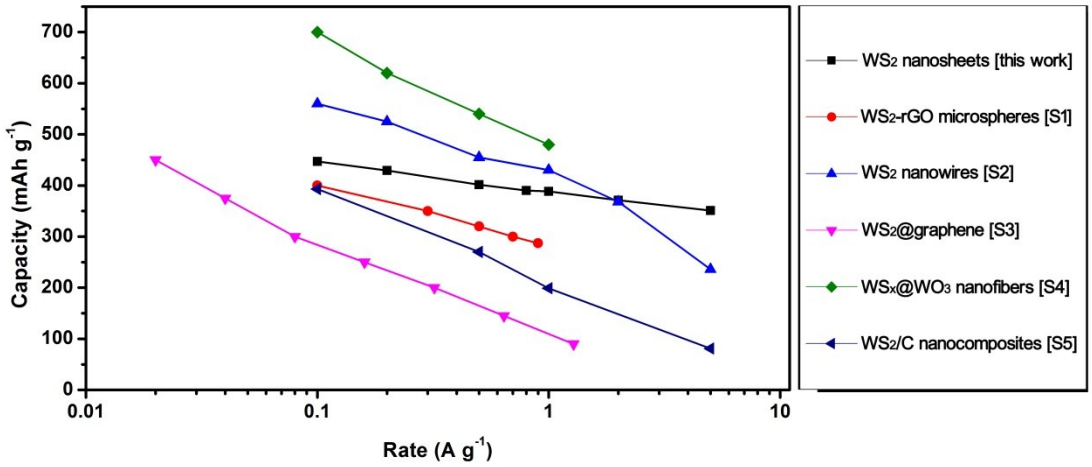

Figure S9. Comparison of rate capability performance for the WS_2 nanosheets electrode with that of WS_2-based sodium-ion battery anodes reported previously (to the best of our knowledge).

Table S1. Comparison of specific capacity and capacity retention at different current densities for the WS_2 nanosheets electrode with those of WS_2-based and other representative TMDs-based sodium-ion battery anodes reported previously.

Materials	**Synthesis method**	**Current density ($A\ g^{-1}$)**	**Cycle number (N)**	**Specific capacity ($mAh\ g^{-1}$)**	**Capacity retention (%)**
WS_2 nanosheets [this work]	*In-situ* chemical vapor deposition	0.1	60	460.8	100
3D WS_2-rGO microspheres [S1]	Spray pyrolysis	0.2	200	334	93
WS_2 nanowires [S2]	Solvothermal & calcination	0.1	50	483.2	79.8
WS_2@graphene nanocomposites [S3]	Hydrothermal approach	0.02	500	329	71.5
WS_x/WO_3 thorn-bush nanofiber [S4]	Electrospinning & post-thermal treatment	0.1	100	585	74
3D porous WS_2/C nanocomposite [S5]	Electrostatic spray deposition	0.5	300	210	84
MoS_2/C flowerlike nanospheres [S6]	Hydrothermal approach	0.67	300	400	76.2
MoS_2/Graphene composite paper [S7]	Vacuum filtration	0.025	20	218	82.3
Vine-like MoS_2 fiber [S8]	Electrospinning	0.1	30	470	63.5
Micro-MoS_2 [S9]	Solid state calcination	0.05	20	400	91
MoS_2 nanoflowers[S10]	Hydrothermal approach	0.2	300	295	100
MoS_2/Graphene composite [S11]	Hydrothermal approach	0.02	100	380	54.3
MoS_2-graphene microspheres [S12]	Spray pyrolysis	0.2	50	480	88
Ultrathin MoS_2 nanosheets [S13]	Ultrasonic exfoliation technique	0.32	100	251	78.4
$MoSe_2$ nanoplates[S14]	Pyrolysis	0.042	50	369	71.9
$FeSe_2$ microspheres [S15]	Hydrothermal approach	1	2000	372	84.2
FeS_2 nanocrystals[S16]	Solution-phase chemical synthesis	1	600	410	50

Core-shell NiSe/C nanospheres [S17]	Hydrothermal approach & calcination	0.1	100	280	70
$CoSe_x$-rGO composite [S18]	Spray pyrolysis	0.3	50	420	80
WSe_2/C composites [S19]	High energy ball milling & calcination	0.2	50	270	91.8

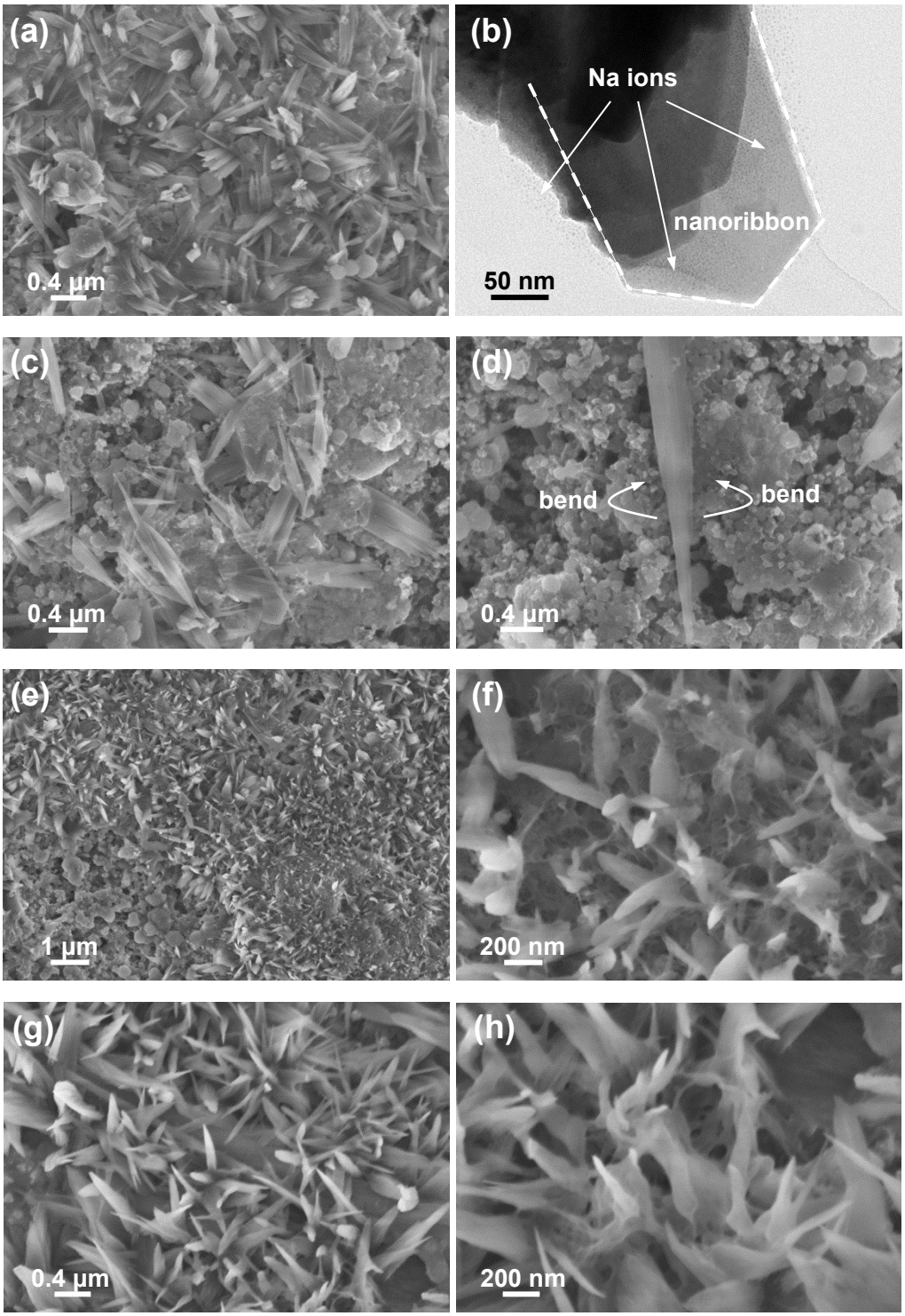

Figure S10. (a)(b) SEM and TEM images of the active materials after the electrode was discharged to 0.4 V at the initial cycle. Typical SEM images with different magnification times of the WS_2 electrodes which were soaked in DMC for 12 h after the electrode was discharged to (c)(d) 0.2 V, (e)(f) 0.005 V and then charged to (g)(h)

3.0 V during the first cycle.

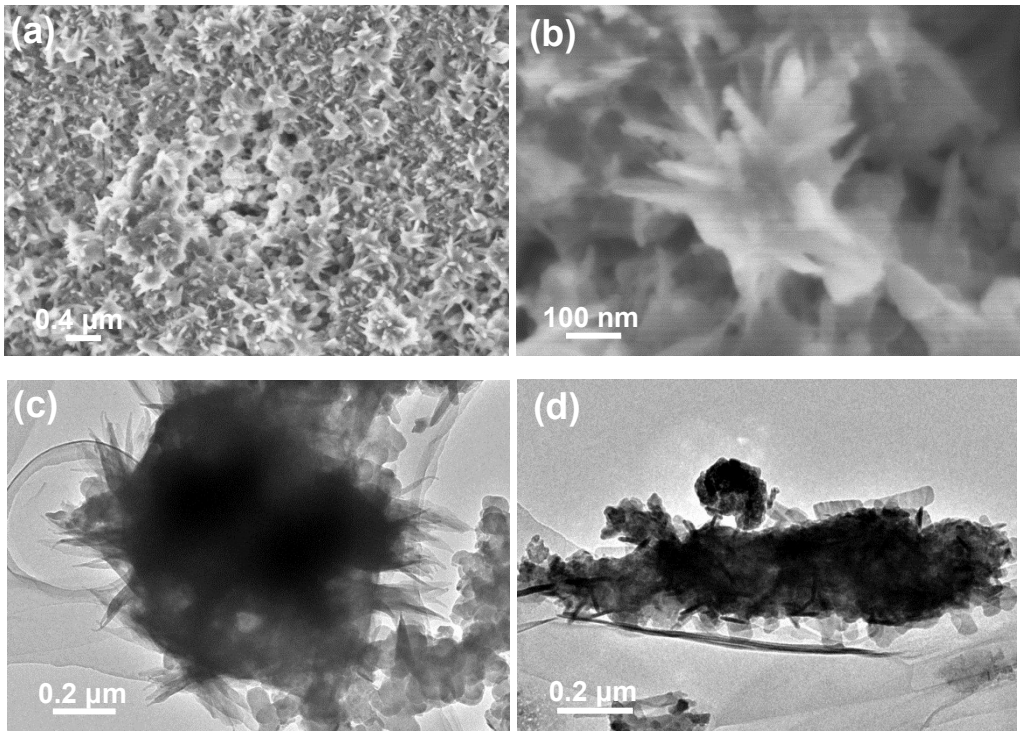

Figure S11. (a)(b) SEM images at the different magnification times of the electrode of WS_2 nanosheets with being soaked in DMC for 12 h to expose active material after the rate test. (c)(d) Typical TEM images of the active materials scratched from the electrode of WS_2 nanosheets after the rate test.

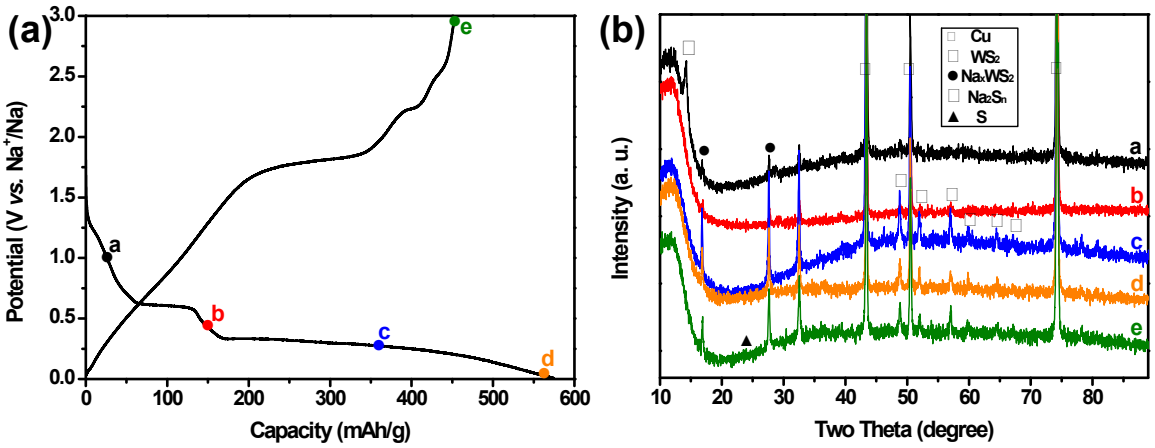

Figure S12. (a) The discharge/charge profiles of the WS_2 nanosheets electrode at 0.1 A g^{-1} from 0.01 to 3.0 V at the first cycle. The letters "a" to "e" denote the different sodiated/desodiated statuses. (b) *Ex-situ* X-ray patterns of WS_2 nanosheets electrodes collected at different discharge/charge statues marked with letters from "a" to "e".

References:

[1] S. H. Choi and Y. C. Kang, *Nanoscale*, 2015, **7**, 3965-3970.

[2] Y. Liu, N. Zhang, H. Kang, M. Shang, L. Jiao and J. Chen, *Chem.—Eur. J.*, 2015, **21**, 11878-11884.

[3] D. Su, S. Dou and G. Wang, *Chem. Commun.*, 2014, **50**, 4192-4195.

[4] W. Ryu, H. Wilson, S. Sohn, J. Li, X. Tong, E. Shaulsky, J. Schroers, M. Elimelech and A. D. Taylor, *ACS Nano*, 2016, **10**, 3257-3266.

[5] C. Zhu, P. Kopold, W. Li, P. A. van Aken, J. Maier and Y. Yu, *J. Mater. Chem. A*, 2015, **3**, 20487-20493.

[6] J. Wang, C. Luo, T. Gao, A. Langrock, A. C. Mignerey and C. Wang, *Small*, 2015, **11**, 473-481.

[7] L. David, R. Bhandavat and G. Singh, *ACS Nano*, 2014, **8**, 1759-1770.

[8] W. H. Ryu, J. Jung, K. Park, S. Kima and I. Kim, *Nanoscale*, 2014, **6**, 10975-

10981.

[9] X. Wang, Y. Li, Z. Guan, Z. Wang and L. Chen, *Chem.—Eur. J.*, 2015, **21**, 6465-6468.

[10] Z. Hu, L. Wang, K. Zhang, J. Wang, F. Cheng, Z. Tao and J. Chen, *Angew. Chem., Int. Ed.*, 2014, **53**, 12794-12798.

[11] X. Xie, Z. Ao, D. Su, J. Zhang and G. Wang, *Adv. Funct. Mater.*, 2015, **25**, 1393-1403.

[12] S. H. Choi, Y. N. Ko, J. Lee and Y. C. Kang, *Adv. Funct. Mater.*, 2015, **25**, 1780-1788.

[13] D. Su, S. Dou and G. Wang, *Adv. Energy Mater.*, 2015, **5**, 1401205.

[14] H. Wang, X. Lan, D. Jiang, Y. Zhang, H. Zhong, Z. Zhang and Y. Jiang, *J. Power Sources*, 2015, **283**, 187-194.

[15] K. Zhang, Z. Hu, X. Liu, Z. Tao and J. Chen, *Adv. Mater.*, 2015, **27**, 3305-3309.

[16] M. Walter, T. Zund and M. V. Kovalenko, *Nanoscale*, 2015, **7**, 9158-9163.

[17] Z. Zhang, X. Shi and X. Yang, *Electrochim. Acta*, 2016, **208**, 238-243.

[18] G. D. Park and Y. C. Kang, *Chem.—Eur. J.*, 2016, **22**, 4140-4146.

[19] Z. Zhang, X. Yang and Y. Fu, *RSC Adv.*, 2016, **6**, 12726-12729.